DOI: 10.1002/chem.200701547

Polar Intermetallic Compounds as Catalysts for Hydrogenation Reactions: Synthesis, Structures, Bonding, and Catalytic Properties of $Ca_{1-x}Sr_xNi_4Sn_2$ ($x = 0.0$, 0.5, 1.0) and Catalytic Properties of Ni_3Sn and Ni_3Sn_2

Viktor Hlukhyy,[a] Fabian Raif,[b] Peter Claus,[b] and Thomas F. Fässler*[a]

Dedicated to Professor Wolfgang A. Herrmann on the occasion of his 60th birthday

Abstract: The potential of polar intermetallic compounds to catalyze hydrogenation reactions was evaluated. The novel compounds $CaNi_4Sn_2$, $SrNi_4Sn_2$, and $Ca_{0.5}Sr_{0.5}Ni_4Sn_2$ were tested as unsupported alloys in the liquid-phase hydrogenation of citral. Depending on the reaction conditions, conversions of up to 21.0% (253 K and 9.0 MPa hydrogen pressure) were reached. The binary compounds Ni_3Sn and Ni_3Sn_2 were also tested in citral hydrogenation under the same conditions. These materials gave conversions of up to 37.5%. The product mixtures contained mainly geraniol, nerol, citronellal, and citronellol. The isotypic stannides $CaNi_4Sn_2$, $Ca_{0.5}Sr_{0.5}Ni_4Sn_2$, and $SrNi_4Sn_2$ were obtained by melting mixtures of the elements in an arc-furnace under an argon atmosphere. Single crystals were synthesized in tantalum ampoules using special temperature modes. The novel structures were established by single-crystal X-ray diffraction. They crystallize in the tetragonal space group $I4/mcm$ with parameters: $a = 7.6991(7)$, $c = 7.8150(8)$ Å, $wR2 = 0.034$, 162 F^2 values, 14 variable parameters for $CaNi_4Sn_2$; $a = 7.7936(2)$, $c = 7.7816(3)$ Å, $wR2 = 0.052$, 193 F^2 values, 15 variable parameters for $Ca_{0.5}Sr_{0.5}Ni_4Sn_2$; and $a = 7.8916(4)$, $c = 7.7485(5)$ Å, $wR2 = 0.071$, 208 F^2 values, 14 variable parameters for $SrNi_4Sn_2$. The $Ca_{1-x}Sr_xNi_4Sn_2$ ($x = 0.0$, 0.5, 1.0) structures can be represented as a stuffed variant of the $CuAl_2$ type by the formal insertion of one-dimensional infinite Ni-cluster chains $[Ni_4]$ into the $Ca(Sr)Sn_2$ substructure. The Ni and Sn atoms form a three-dimensional infinite $[Ni_4Sn_2]$ network in which the Ca or Sr atoms fill distorted octagonal channels. The densities of states obtained from TB-LMTO-ASA calculations show metallic character for both compounds.

Keywords: calcium · crystal structure · hydrogenation catalysts · intermetallic compounds · strontium

Introduction

Intermetallic compounds comprise two or more metals that crystallize to produce a structure which differs from those of the constituent metals. The search for polar intermetallic compounds with a well-defined stoichiometry and which are also catalytically active is a high challenge because, on the one hand, the combination of various metals might be able to substitute expensive platinum group metal catalysts as currently used, for example, for the selective hydrogenation of α,β-unsaturated aldehydes. Usually, the metal component is deposited on support materials (e.g. SiO_2, Al_2O_3, TiO_2, carbon); however, the catalytic behavior is often influenced by the latter for which the SMSI (strong metal-support interaction) effect is a prominent example. On the other hand, knowledge of the intrinsic catalytic properties of well-defined alloy catalysts (i.e. of non-supported metals occupying well-defined sites in the crystal structure) aids in correlating this property with the electronic structures of the compounds. The use of non-supported bulk materials is a prerequisite for such studies of the bulk catalytic properties of the alloys. The conversion rate will be certainly lower than that of the supported catalyst owing to the smaller active surface area. Certainly, surface effects are also important and must be considered; however, the systematic study of

[a] Dr. V. Hlukhyy, Prof. Dr. T. F. Fässler
Department Chemie, Technische Universität München
Lichtenbergstrasse 4, 85748 Garching (Germany)
Fax: (+49) 89-289-13186
E-mail: thomas.faessler@lrz.tu-muenchen.de

[b] Dipl.-Ing. F. Raif, Prof. Dr. P. Claus
Ernst Berl-Institut für Technische und Makromolekulare Chemie,
Fachbereich Chemie, Technische Universität Darmstadt
Petersenstrasse 20, 64287 Darmstadt (Germany)

Supporting information for this article is available on the WWW under http://www.chemeurj.org/ or from the author.

well-defined intermetallic compounds is an alternative approach and is especially suited to the search of new catalysts and only a few attempts have been made to correlate the bulk properties of unsupported, well-defined alloys with their catalytic activity.[1]

To find novel intermetallic compounds that can be used as hydrogenation catalysts, we started to investigate binary and ternary phase diagrams of more electropositive metals, such as alkaline-earth metals (AE), a late transition metal, and Group 14 element as components. Late transition metals are often present during catalytic hydrogenation reactions and the Group 14 element Sn often serves as promotor. The introduction of electropositive metals has not only a drastic influence on the ligand effect (i.e. the electronic influence of neighboring atoms on the base metal atom) in a multicomponent catalyst, but it also influences the Fermi level by a partial charger transfer from the alkaline-earth metal to the other metals involved. We recently discovered the catalytic properties of (unsupported) intermetallic Mg_2Sn[2] and $MgCo_6Ge_6$,[3] both of which exhibited remarkable activity in the hydrogenation of citral to the allylic alcohols geraniol and nerol (products of C=O group hydrogenation). Intermetallics with such compositions have not yet been regarded as catalytically active materials.

Polar intermetallic compounds are intermediate between the saltlike Zintl phases and solid solutions because they are well-defined with respect to each individual atomic position of the structure and possess some degree of directional bonding. According to the Zintl–Klemm concept, the Zintl phases are in agreement with the (8−N) electron-counting rule and are thus valence compounds. In the case of polar transition-metal-rich intermetallics, it is not possible to use such electron-counting rules; however, a negatively charged polyanionic partial structure can be presumed in most cases. We have now extended our investigations on such polar intermetallics with respect to the nickel-based systems. Here we report our results in the Ni-rich part of the phase diagram Ca-Ni-Sn and Sr-Ni-Sn and, for comparison, an examination of the binary phases Ni_3Sn-LT and Ni_3Sn_2-HT.[4] At the start of our investigations, only three compounds in those systems had been reported: $Ca_7Ni_4Sn_{13}$[5] $SrNiSn_2$, and $SrNiSn_3$[6]. Previous investigations revealed that in all *AE*-*T*-Sn compounds (*AE* = Ca, Sr, Ba; *T* = transition metal), the transition metal and tin atoms build a two- or three-dimensional $[T_xSn_y]$ polyanion, in which the Ca, Sr, or Ba atoms separate the polyanionic layers or fill channels within the polyanions.[7–14] The structural features of the *T*-Sn network are reminiscent of the catalyst/co-catalyst scenario of a bimetallic system. In contrast to calcium, strontium, and barium and owing to its small size, magnesium often exhibits significant mixing with tin atom sites and might induce a change of the structure type in a series of solid solutions.[15–18] Therefore, Mg-containing compounds were not investigated at this point.

With strontium and calcium as the electropositive components we obtained the structurally related stannides $CaNi_4Sn_2$, $SrNi_4Sn_2$, and $Ca_{0.5}Sr_{0.5}Ni_4Sn_2$ that contain a three-dimensional $[Ni_4Sn_2]$ network. The preparation and crystal chemistry as well as their catalytic properties are reported herein. A brief account of this work has been presented at a conference.[19]

Results and Discussion

Synthesis: The compounds Ni_3Sn, Ni_3Sn_2, $CaNi_4Sn_2$, $SrNi_4Sn_2$, and $Ca_{0.5}Sr_{0.5}Ni_4Sn_2$ were synthesized by high-temperature fusion of the elements in the stoichiometric ratio. During arc-melting of the ternary and quasiternary phases, small amounts of the calcium and strontium were lost owing to the high vapor pressure of these components. Therefore, phases with 1:4:2 compositions contained very small amounts of binary Ni_3Sn and Ni_3Sn_2. Attempts to synthesize purer samples failed.

Structure description of $SrNi_4Sn_2$ and $CaNi_4Sn_2$: The structure determinations from single-crystal X-ray diffraction experiments showed that the structures consist of a three-dimensional NiSn framework with quasi-tetra and -octagonal channels along the *c* direction. The latter host the Sr or Ca atoms, which are consequently aligned along *c*. The discussion is given for *AE* = Ca, but is equally valid for *AE* = Sr and mixture Ca/Sr. Crystal data and details of the structure refinements as well as atomic parameters and important interatomic distances are given in Tables 1–3. A projection of the $CaNi_4Sn_2$ structure along the *z* axis is presented in Figure 1a. The skeletal structure of the atoms forming the tetragonal channels is a one-dimensional Ni-atom strand shown as solid black lines in Figure 1b. The Ni–Ni distances in the skeletal chain are relatively short and range from 2.52 to 2.58 Å for $CaNi_4Sn_2$ and from 2.51 to 2.54 Å for $SrNi_4Sn_2$, and are thus close to the Ni–Ni distance of 2.49 Å in fcc nickel.[34] The Ni partial structure can be described as a fusion of six-membered Ni rings with exclusively boat conformation and can also be illustrated as a polymerization of Ni_8 cubes as shown in Figure 1c. Interestingly, a similar one-dimensional structure motif occurs in $Ca_7Co_8Sn_{25}$ ($Pr_3Rh_4Sn_{13}$ type).[35] However, the strands in $Ca_7Co_8Sn_{25}$ consist of Sn atoms and are stacked perpendicularly to each other in the three directions of cubic symmetry. In $CaNi_4Sn_2$, the tin atoms are located above each center of the boat-type Ni_6 unit to form six Sn–Ni contacts with 2.64 and 2.63 Å. The Sn atoms stitch these Ni chains [d(Sn–Ni) = 2.55 Å] to produce a three-dimensional infinite $[Ni_4Sn_2]$ network. The Ni–Sn distances in both compounds cover the range from 2.55 to 2.64 Å in $CaNi_4Sn_2$ and from 2.60 to 2.66 Å in $SrNi_4Sn_2$. These distances compare well with the sum of the covalent radii of 2.63 Å,[36] indicating strong Ni–Sn interactions in these two stannides. Such Ni–Sn distances are also typical for stannides with other structures, such as $Ca_7Ni_4Sn_{13}$,[5] $SrNiSn_3$, and $BaNiSn_3$,[6] $MgNi_2Sn$.[37] The $[Ni_4Sn_2]$ network has only Ni–Ni and Ni–Sn, but no Sn–Sn contacts. The distance between nearest Sn atoms is 3.46 Å in $CaNi_4Sn_2$ and 3.59 Å in $SrNi_4Sn_2$ and are much longer than

Table 1. Crystal data and structure refinement of $CaNi_4Sn_2$, $Ca_{0.5}Sr_{0.5}Ni_4Sn_2$, and $SrNi_4Sn_2$ (space group $I4/mcm$, $Z=4$).

empirical formula	$CaNi_4Sn_2$	$Ca_{0.5}Sr_{0.5}Ni_4Sn_2$	$SrNi_4Sn_2$
formula weight	512.30	536.07	559.84
unit cell dimensions [Å] (powder data)			
a	7.6991(7)	7.7936(2)	7.8916(4)
c	7.8150(8)	7.7816(3)	7.7485(3)
V [Å^3]	463.2	472.7	482.6
ρ_{calcd} [g cm^{-3}]	7.346	7.533	7.706
absorption coefficient [mm^{-1}]	30.1	31.9	36.2
$F(000)$	928	964	1000
detector distance [mm]	70	100	70
exposure time [min]	5	1	5
ω range [°]; increment [°]	0–180; 1.0	0–180; 1.0	0–180; 1.0
integr. param. A, B, EMS	12; 2; 0.015	14.0; 3.0; 0.020	14.0; 4.0; 0.010
θ range for data collection [°]	4–27.5	4–30	4–30
range in hkl	$-6\le h\le 7$	$-10\le h\le 10$	$-10\le h\le 11$
	$0\le k\le 9$,	$-10\le k\le 10$	$0\le k\le 10$
	$0\le l\le 10$	$-10\le l\le 10$	$0\le l\le 10$
total no. of reflns	267	4127	664
independent reflns (R_{int})	160 (0.0094)	193 (0.0933)	208 (0.0721)
reflns with $I>2\sigma(I)$; (R_σ)	142 (0.0133)	172 (0.0237)	196 (0.0421)
transmission, max./min.	2.55	3.59	7.71
no. of parameters	160/14	193/15	208/14
goodness-of-fit on F^2	0.979	1.172	1.228
final R indices [$I>2\sigma(I)$]			
$R1$	0.015	0.026	0.029
$wR2$	0.034	0.052	0.070
R indices (all data)			
$R1$	0.019	0.033	0.030
$wR2$	0.034	0.054	0.071
extinction coefficient	0.0006(1)	0.0014(3)	0.059(3)
largest diff. peak and hole [e Å^{-3}]	0.71/−0.57	1.38/−1.41	2.66/−1.52

Table 2. Atomic parameters and isotropic displacement parameters (Å$^3\times 10^3$) of $CaNi_4Sn_2$, $SrNi_4Sn_2$, and $Ca_{0.5}Sr_{0.5}Ni_4Sn_2$ compounds.

Atom	Wyckoff position	Occup. [%]	x	y	z	U_{eq}
Ca	4*a*	100	0	0	1/4	21(1)
Sn	8*h*	100	0.34087(5)	1/2−x	0	17(1)
Ni	16*l*	100	0.36076(6)	1/2−x	0.33504(8)	18(1)
Sr	4*a*	100	0	0	1/4	9(1)
Sn	8*h*	100	0.33918(6)	1/2−x	0	9(1)
Ni	16*l*	100	0.36444(10)	1/2−x	0.33803(10)	11(1)
Ca/Sr	4*a*	51(1)/49(1)	0	0	1/4	16(1)
Sn	8*h*	100	0.34011(7)	1/2−x	0	15(1)
Ni	16*l*	100	0.36254(10)	1/2−x	0.33669(12)	17(1)

bonding Sn–Sn distances in α-Sn (2.81 Å) and β-Sn (4× 3.02 Å; 2×3.18 Å).[34] Ca–Ni and Sr–Ni contacts are 3.05 and 3.14 Å and are thus a bit longer than the sum of Pauling's single-bond radii of 2.98 and 3.13 Å for $CaNi_4Sn_2$ and $SrNi_4Sn_2$, respectively. All interatomic distances in the $Ca_{0.5}Sr_{0.5}Ni_4Sn_2$ compound lie in a range between those of $CaNi_4Sn_2$ and $SrNi_4Sn_2$.

The NiSn substructure resembles the $CeNi_4Sn_2$[25] structure in which the Ni and Sn atoms form a one-dimensional infinite cluster chain [Ni_4Sn_2] with weaker Ni–Sn contacts (2.75 Å) between the chains.

Structure relationships: From a crystallographic point of view, the Ca-Sn sublattice in $CaNi_4Sn_2$ can be derived from the tetragonal $CuAl_2$-type[37] by replacing Cu by Ca atoms and Al by Sn atoms to form the hypothetical binary stannide "$CaSn_2$" (Figure 2). In the $CuAl_2$ type, the Al (Sn) atoms form layers of planar square-triangle 3^2434 nets oriented perpendicular to the c axis. The layers are stacked so that the square units of two layers form antiprisms which are centered by Cu (Ca) atoms and tetrahedral edge-sharing Al_4 (Sn_4) units (Figure 2a). Ni atoms are inserted above the tetrahedral faces of the Sn_4 units to form a so-called tetraederstern and leading to a one-dimensional atom arrangement along c, as emphasized in Figure 1b. There is also a strong relation to the SiV_4Sb_2-type,[38] which is an ordered variant of U_6Mn (Figure 2c).[39] In SiV_4Sb_2, the $CuAl_2$-type "$SiSb_2$" sublattice (Wyckoff positions 4*a*, 8*h*) is stuffed with an infinite one-dimensional cluster chain of V atoms (Wyckoff position 16*k*). Similar to the Sb atoms, the V atoms form a one-dimensional chain of square-face-sharing antiprisms; however, these [V_4] chains are quite different from the [Ni_4] in the $CaNi_4Sn_2$ structure. In the SiV_4Sb_2 structure, the V atoms are inserted into the layers of the Sb atoms, whereas the Ni atoms in the $CaNi_4Sn_2$ structure are located between Sn atoms along the c direction. Consequently, SiV_4Sb_2 has a smaller c/a ratio of 0.477, in contrast to $CaNi_4Sn_2$ with a c/a ratio of 1.015 and to the $CuAl_2$ "matrix" with a c/a ratio of 0.804. From another point of view, the $CaNi_4Sn_2$ structure can be considered as a ternary defective variant of Cr_5B_3 ($I4/mcm$, $c/a=1.949$; Figure 3).[4] In the Cr_5B_3 structure, four Cr atoms form a distorted tetrahedron. The Cr atoms of the tetrahedral units have, however, no intercluster contacts along the c axis. Pairs of B atoms connect the four-atom clusters, which is very similar to the pairs of Sn atoms in $CaNi_4Sn_2$. Whereas in the structure of $CaNi_4Sn_2$ the Ca atoms (4*a* site) fill the channels of the three-dimensional infinite [Ni_4Sn_2] network, similar channels, formed by the [Cr_4B_2] network in the Cr_5B_3 structure, are occupied by two types of atoms: B1 (4*a* site) and Cr1 (4*c* site). This addition of Cr1 atoms into the channels causes a significant increase in the c lattice parameter and stretches the [Cr_4] chains (16*l* site) and, consequently, the [Cr_4]-atom units are not interconnected (Figure 3b). Interestingly, the packing of La and

Table 3. Interatomic distances [Å] in the $CaNi_4Sn_2$, $Ca_{0.5}Sr_{0.5}Ni_4Sn_2$, and $SrNi_4Sn_2$ compounds.[a]

	$CaNi_4Sn_2$	$Ca_{0.51}Sr_{0.49}Ni_4Sn_2$	$SrNi_4Sn_2$
Ni–Ni	2.523 (2×)	2.532 (2×)	2.537 (2×)
Ni–Ni	2.578 (1×)	2.542 (1×)	2.510 (1×)
Ni–Ni	2.754 (1×)	2.824 (1×)	2.896 (1×)
Ni–Ni	3.032 (1×)	3.030 (1×)	3.026 (1×)
Ni–Sn	2.546 (1×)	2.570 (1×)	2.596 (1×)
Ni–Sn	2.627 (1×)	2.632 (1×)	2.634 (1×)
Ni–Sn	2.639 (2×)	2.649 (2×)	2.662 (2×)
Ni–Ca(Sr)	3.051 (2×)	3.096 (2×)	3.143 (2×)
Ca(Sr)–Ni	3.051 (8×)	3.096 (8×)	3.143 (8×)
Ca(Sr)–Sn	3.494 (2×)	3.516 (2×)	3.539 (2×)
Ca(Sr)–Ca(Sr)	3.908 (2×)	3.891 (2×)	3.874 (2×)
Sn–Ni	2.546 (2×)	2.570 (2×)	2.596 (2×)
Sn–Ni	2.627 (2×)	2.632 (2×)	2.634 (2×)
Sn–Ni	2.639 (4×)	2.649 (4×)	2.662 (4×)
Sn–Sn	3.465 (1×)	3.525 (1×)	3.590 (1×)
Sn–Ca(Sr)	3.494 (4×)	3.516 (4×)	3.539 (4×)

[a] Standard deviations are all equal or less than 0.002 Å.

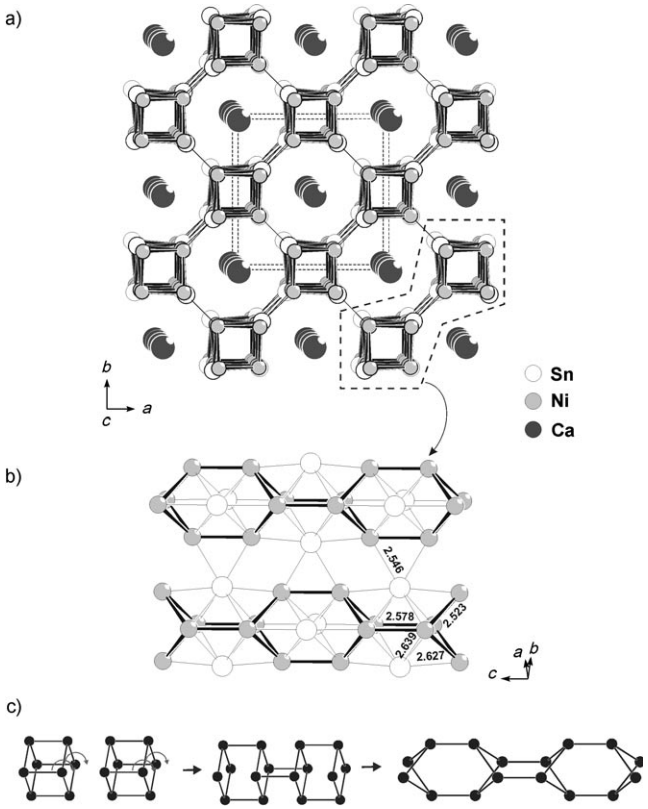

Figure 1. a) Projection of the $CaNi_4Sn_2$ structure along the tetragonal axis. A second view of the section marked with dashed lines is shown in Figure 1b. b) Fragment of the three-dimensional infinite $[Ni_4Sn_2]$ network. Two one-dimensional infinite cluster chains $[Ni_4]$ are stitched by Sn atoms into a 3D infinite $[Ni_4Sn_2]$ network. Ni–Ni and Ni–Sn bonds are drawn by thick and thin lines, respectively. Some general bonds are given. Interatomic distances are in Å and refer to $CaNi_4Sn_2$ (Table 3). c) Topological transformation from a linear assembly of hypothetical Ni_8 cubes to the Ni polymer in $CaNi_4Sn_2$.

Ge atoms in the channels of the Cr_5B_3-type is retained in the La_3GeIn_4 structure (*I*4/*mcm*, $c/a = 1.398$, ordered variant of the Cr_5B_3),[40] but the corresponding In_4 tetrahedra (16*l* site) of the $[In_4La_2]$ strands are strongly distorted and are transformed to butterflies without In–In contacts along the *c* axis.

Figure 4 summarizes the two relationships with emphasis on the additional atomic positions in $CaNi_4Sn_2$ and Cr_5B_3 structures. Therefore, $CaNi_4Sn_2$ forms an intermediate structure between the binary $CuAl_2$ and Cr_5B_3 structure types.

It is interesting to note that by changing the smaller Ca atom to a bigger Sr, we observed an increase in the *a* lattice parameter and a decrease in the *c* parameter: a *c*/*a* ratio of 1.015, 0.998, and 0.982 was obtained for $CaNi_4Sn_2$, $Ca_{0.5}Sr_{0.5}Ni_4Sn_2$, and $SrNi_4Sn_2$, respectively. The same effect has also been observed in the series of $RENi_4Sn_2$ compounds,[25] and in other structures containing "channels", such as $CaCu_5$.[41]

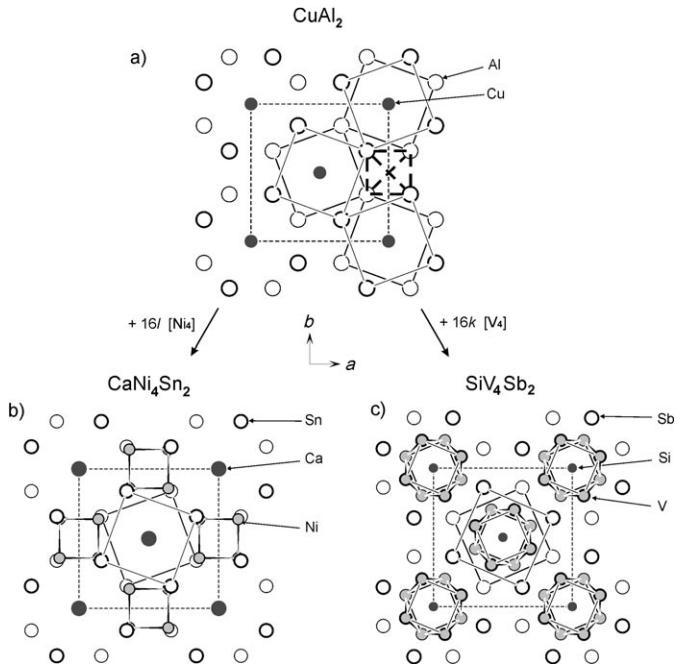

Figure 2. $CaNi_4Sn_2$ and SiV_4Sb_2 structures as derivatives of $CuAl_2$. Projections of the structures are drawn along the tetragonal axis. a) $CuAl_2$-type emphasizing square antiprisms and tetrahedra. b) Insertion of Ni atoms in a "$CaSn_2$" sublattice, c) Insertion of V atoms in a "$SiSb_2$" sublattice.

Chemical bonding: The chemical bonding in $CaNi_4Sn_2$ and $SrNi_4Sn_2$ was investigated by TB-LMTO-ASA[31] band-structure calculations. We confine our discussion of the bonding interactions to $CaNi_4Sn_2$ because the density of states

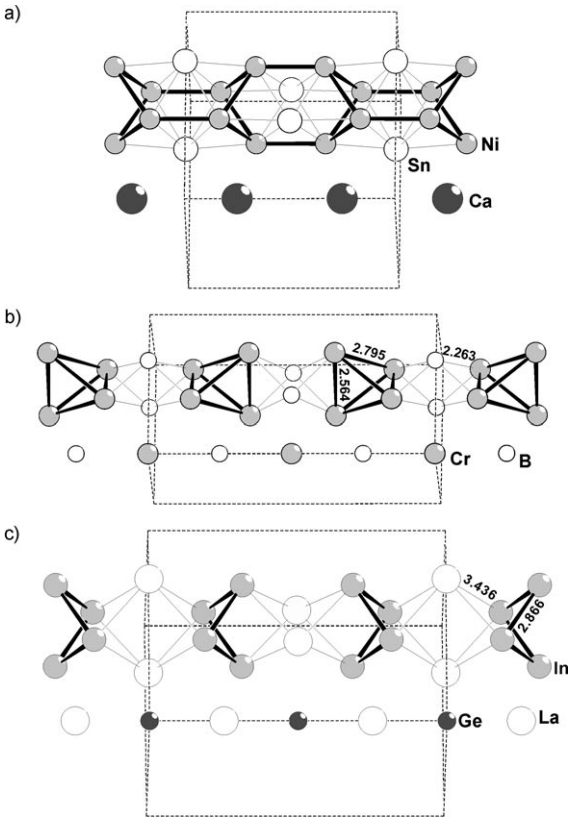

Figure 3. Comparison of the fragments of $[X_4Y_2]$ infinite cluster chains in: a) $CaNi_4Sn_2$, b) Cr_5B_3, and c) La_3GeIn_4. Some general bonds are given.

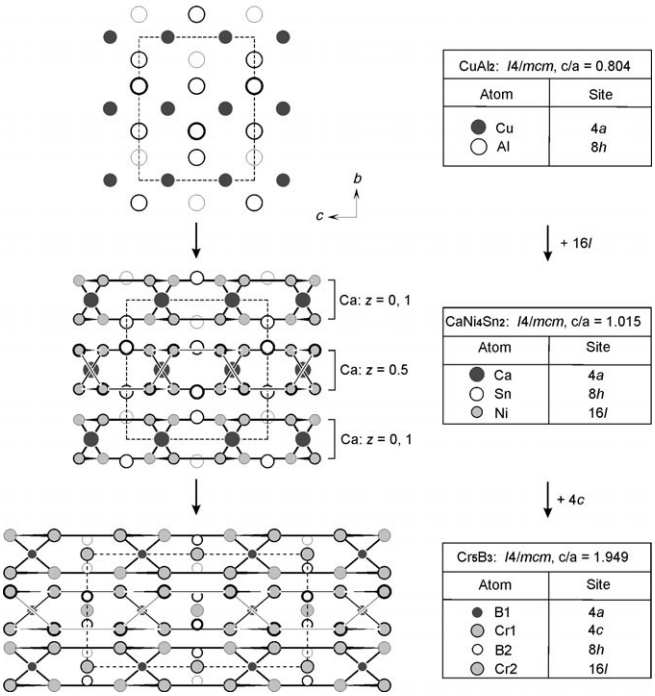

Figure 4. The relationship between three structures: $CuAl_2$ (top), $CaNi_4Sn_2$ (middle), and Cr_5B_3 (bottom). Atoms in the 16*l* site are bonded between themselves.

(DOS) of $SrNi_4Sn_2$ is essentially of the same type as in $CaNi_4Sn_2$. Total and partial DOS plots of $CaNi_4Sn_2$ are shown in Figure 5. No energy gap is discernable at the

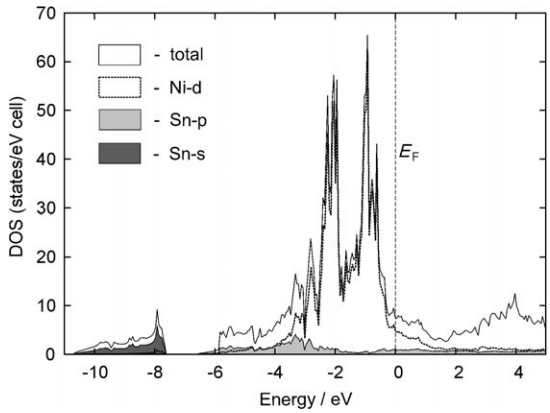

Figure 5. Total and projected DOS curves for $CaNi_4Sn_2$. The energy zero is taken at the Fermi level.

Fermi level E_F, which indicates that the compounds have a metallic character. The DOS in the valence region has significant nickel character with tin levels contributing from −5.8 eV up to the Fermi level. The states below −8 eV are essentially from tin 5s orbitals, whereas the large peaks around −0.3 to −3 eV mainly arise from nickel 3d levels, indicating that there is no significant charge transfer from or to Ni atoms (d^{10} electron configuration). Strong hybridization of nickel and tin orbitals over the entire energy range becomes evident in the partial DOS curves in Figure 5.

For a more quantitative bonding analysis we performed crystal orbital Hamilton populations (COHP),[32] which provide a quantitative measure of the bonding strength. The strongest bonding interactions were found for the three shortest Ni–Sn contacts (Figure 6a), followed by the 3 shortest Ni–Ni contacts (Figure 6b). In contrast to the Ni–Sn contacts, in which mainly bonding states are filled, antibonding interactions also appear in the Ni–Ni COHP curves, a result which is not unusual given that Ni is electron-rich. The Ca–Ni and Ca–Sn interactions are of a bonding nature, but are quantitatively less important (see the Supporting Information.).

These results fit well with the description as a $[Ni_4Sn_2]$ network. The bonds within the network are stronger than those between the network and the calcium atoms.

In view of Pauling's electronegativities of 1.00, 0.95, 1.91, and 1.96 for calcium, strontium, nickel, and tin, respectively, and in agreement with the LMTO calculations, the calcium (strontium) atoms are assumed to have transferred their valence electrons to the nickel and tin atoms. In emphasizing the Ni–Ni and Ni–Sn bonding, electron counting can, to a first approximation, be written as $Ca^{2+}[Ni_4Sn_2]^{2-}$ (or $Sr^{2+}[Ni_4Sn_2]^{2-}$). However, weak Ca(Sr)–Ni contacts also exist in $Ca(Sr)Ni_4Sn_2$. This seems to weaken the concept of their de-

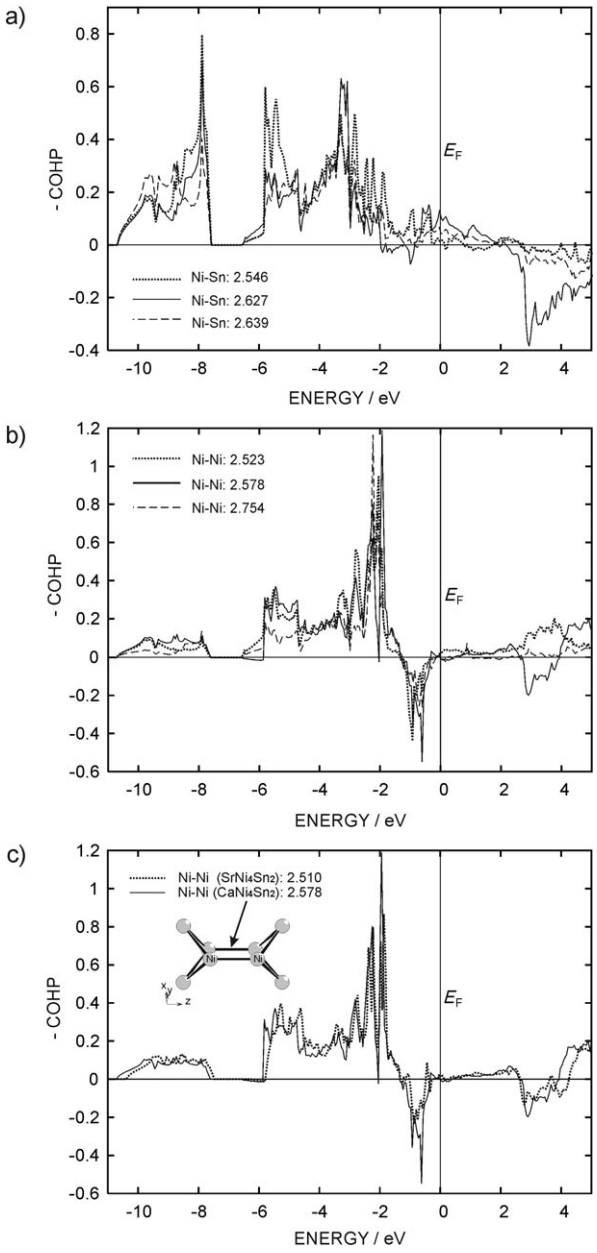

Figure 6. COHP curves for the a) shortest Ni–Sn, b) Ni–Ni contact in $CaNi_4Sn_2$. c) Comparison of the Ni–Ni contacts in $CaNi_4Sn_2$ and $SrNi_4Sn_2$. Distances are given in Å.

scription as a polyanion, but justifies their characterization as *polar* intermetallic compounds.

Catalytic activity and selectivity: The catalytic properties of the alloys were studied using the hydrogenation of citral (3,7-dimethyl-2,6-octadienal) as a test reaction. This α,β-unsaturated aldehyde can be hydrogenated at three unsaturated bonds, including conjugated C=C and C=O groups as well as an isolated C=C bond. The selective hydrogenation of citral affords industrially important products, for example, for the perfumery and flavoring industry. C=C bond hydrogenation leads to citronellal, whereas hydrogenation of its conjugated C=O bond yields unsaturated alcohols in the *cis* and *trans* forms (geraniol and nerol). The additional insertion of hydrogen into these intermediates, under certain reaction conditions and depending on the catalyst type, leads to citronellol, dihydrocitronellal, and 3,7-dimethyloctanal.

The hydrogenation of citral was catalyzed with the unsupported, low surface area $CaNi_4Sn_2$, $SrNi_4Sn_2$, and $Ca_{0.5}Sr_{0.5}Ni_4Sn_2$ compounds as catalysts. Citral conversion increases in the order $SrNi_4Sn_2$, $Ca_{0.5}Sr_{0.5}Ni_4Sn_2$, and $CaNi_4Sn_2$ from 10.5, 16.6, to 21.0%, employing the samples respectively, at a temperature of 453 K and a hydrogen pressure of 9.0 MPa (Table 4). Under these reaction conditions, $CaNi_4Sn_2$ achieved a remarkable selectivity of 41% in the desired products geraniol and nerol, which means that these intermetallic compounds can be regarded as chemoselective hydrogenation catalysts. The intermetallic compound $MgCo_6Ge_6$ reached 48% selectivity under comparable reaction conditions, which lies in the same order of magnitude.[3] Under the desired reaction conditions, $SrNi_4Sn_2$ and $Ca_{0.5}Sr_{0.5}Ni_4Sn_2$ gave a selectivity of 19% for the reaction to geraniol and nerol. X-ray analysis and Rietveld refinement of the ternary samples showed that they contained very small amounts of the binary phases Ni_3Sn and Ni_3Sn_2. It cannot be excluded that the catalytic properties of the (pseudo-)ternary compounds $CaNi_4Sn_2$, $SrNi_4Sn_2$, and $Ca_{0.5}Sr_{0.5}Ni_4Sn_2$ are influenced by small amounts of the binary compounds Ni_3Sn and Ni_3Sn_2. For this reason, the low surface area Ni_3Sn and Ni_3Sn_2 compounds were used under the same reaction conditions. The Ni_3Sn and Ni_3Sn_2 phases reached conversions of 12.7 and 37.5%, the latter is comparable to supported metal catalysts.[42] High selectivities to the unsaturated alcohols geraniol and nerol of 50 and 71% were reached. Samples of $CaNi_4Sn_2$, $SrNi_4Sn_2$, $Ca_{0.5}Sr_{0.5}Ni_4Sn_2$, Ni_3Sn, Ni_3Sn_2, and $MgCo_6Ge_6$ yielded comparable geraniol/nerol product ratios of ≈2. An interesting property of a polar intermetallic compound is catalytic for-

Table 4. Catalytic results of citral hydrogenation over $CaNi_4Sn_2$, $Ca_{0.5}Sr_{0.5}Ni_4Sn_2$, $SrNi_4Sn_2$, Ni_3Sn, and Ni_3Sn_2 at 453 K.

	$CaNi_4Sn_2$[a]	$Ca_{0.5}Sr_{0.5}Ni_4Sn_2$[a]	$SrNi_4Sn_2$[a]	Ni_3Sn[a]	Ni_3Sn_2[a]
citral conversion [%]	21.0	16.6	10.5	37.5	12.7
selectivity [%]					
geraniol + nerol[b]	41	19	19	50	71
citronellal[c]	22	12	2	37	15
citronellol[d]	11	1	16	9	14
other products[e]	26	68	63	4	0
geraniol/nerol ratio	2.3	2.1	1.7	2.1	2.4
(geraniol + nerol)/(citronellal + citronellol) ratio	1.2	1.5	1.1	1.1	2.4

[a] $m_{cat}=100$ mg, $c_{Citral}=0.58$ mol L^{-1}, $pH_2=9.0$ MPa, $t=150$ min. [b] (*trans* + *cis*) product of C=O group hydrogenation. [c] Product of conjugated C=C bond hydrogenation. [d] Product of the consecutive hydrogenation of geraniol, nerol, and citronellal. [e] Isopulegol, menthol, and non-identified products.

mation of the desired unsaturated alcohols at a comparable level as indicated, for example, by the product ratio of (geraniol + nerol)/(citronellal + citronellol). These calculated ratios for the $CaNi_4Sn_2$, $SrNi_4Sn_2$, and $Ca_{0.5}Sr_{0.5}Ni_4Sn_2$ samples were 1.2, 1.1, and 1.5, respectively, whereas values of 1.1, 2.4, and 4.6 were reached with the Ni_3Sn, Ni_3Sn_2, and $MgCo_6Ge_6$ samples, respectively.

Conclusion

The total amount of citral conversion increases from $SrNi_4Sn_2$, Ni_3Sn_2, $Ca_{0.5}Sr_{0.5}Ni_4Sn_2$, $CaNi_4Sn_2$ to Ni_3Sn. Ni_3Sn_2 and Ni_3Sn exhibited the highest selectivity for geraniol and nerol, followed by ternary $CaNi_4Sn_2$. Therefore, the catalytic reaction sensitively depends on the composition, but did not benefit from the increase in polarity of the intermetallic compound by introduction of an alkaline-earth metal. Interestingly, the phase with the lowest Ni content shows the best selectivity. However, these intermetallic compounds, so far not known in catalysis, can be regarded as chemoselective hydrogenation catalysts. The formation of allylic alcohols (geraniol and nerol) rather than the saturated aldehyde (citronellal) is in agreement with the improved selectivity towards C=O hydrogenation of bimetallic (supported) catalysts, for which Sn seems to be the second metal of choice for modifying the base metal. Ni_3Sn_2 shows a rather similar DOS at E_F as $CaNi_4Sn_2$ with a small peak at the Fermi level and both compounds show the highest selectivity of the system under investigation here. As in the case of $CaNi_4Sn_2$, the peak at E_F correlates with Ni–Sn bonding states. Since there are considerable Ni and Sn contributions at the Fermi level E_F with mainly Ni–Sn bonding character, those states are considered to be relevant for the hydrogenation process.

Experimental Section

Syntheses: Starting materials for the preparation of $CaNi_4Sn_2$, $SrNi_4Sn_2$, and $Ca_{0.5}Sr_{0.5}Ni_4Sn_2$ were ingots of calcium and strontium (ChemPur), nickel wire (∅1 mm, Johnson-Matthey), and tin teardrops (ChemPur), all with stated purities better than 99.5%. The calcium pieces were first arc-melted to small buttons. The premelting procedure strongly reduces shattering of the calcium during the exothermic reaction with nickel and tin. Pieces of the calcium (or strontium), pieces of nickel wire, and pieces of the tin teardrops were mixed in the ideal 1:4:2 atomic ratios and arc-melted. Each pellet was remelted three times in order to ensure homogeneity. All manipulations were performed in an Argon-filled glove box.

After the arc-melting procedure well-shaped single crystals suitable for a structure determination were only detected in the $Ca_{0.5}Sr_{0.5}Ni_4Sn_2$ sample, while the $CaNi_4Sn_2$ and $SrNi_4Sn_2$ samples remained polycrystalline. Therefore, crystal growth for $CaNi_4Sn_2$ and $SrNi_4Sn_2$ was then performed with a special temperature mode. The sample was crushed, powdered, and cold-pressed to a pellet. The pellet was placed in a tantalum container and enclosed in an evacuated silica tube, which was placed in a muffle furnace. The samples were first heated at 1270 K within 6 h and held at that temperature for 5 h. The temperature was then lowered at a rate of 6 K h^{-} to 970 K, then at a rate of 24 K h^{-} to 670 K, and finally cooled to room temperature within 3 h. After cooling to room temperature, the samples could easily be separated from the tantalum crucibles. No reaction of the samples with the crucible material was detected. All samples are gray and stable with respect to air and moisture as compact buttons and as fine-grained powders. Single crystals with a metallic luster were suitable for X-ray investigations.

The binary Ni_3Sn-LT and Ni_3Sn_2-HT phases were synthesized from the elements by arc-melting techniques. Pieces of nickel wire and pieces of the tin teardrops were mixed in 3:1 and 3:2 atomic ratios and arc-melted. The product buttons were turned over and remelted several times in order to ensure homogeneity. After arc-melting, gray polycrystalline products were obtained.

X-ray investigations and structure refinements: The purity of the samples was checked with a STOE STADI P powder diffractometer with $Cu_{K\alpha1}$ radiation. The tetragonal lattice parameters (Table 1) were obtained from least-squares fits of the powder data for $CaNi_4Sn_2$ and $SrNi_4Sn_2$, while a cubic cell was found for $Ca_{0.5}Sr_{0.5}Ni_4Sn_2$ (owing to the close values of the *a* and *c* parameters). The tetragonal lattice parameters were only established after careful analysis of the $Ca_{0.5}Sr_{0.5}Ni_4Sn_2$ powder diffractogram by Rietveld refinement with the Fullprof Suite[20] (Table 1). The Rietveld refinement showed that the samples contained not only the main phase, but also very small amounts of the binary phases: Ni_3Sn-LT (1%) and Ni_3Sn_2 (5%) in $CaNi_4Sn_2$, Ni_3Sn_2 (7%) in $Ca_{0.5}Sr_{0.5}Ni_4Sn_2$, and Ni_3Sn_2 (3%) and a very small amount of an unknown phase in $SrNi_4Sn_2$. The linear increase in the lattice parameters with x for $x=0$, 0.5, and 1 confirm a degree of substitution identical to that determined by single-crystal and powder X-ray studies. The Ni_3Sn-LT and Ni_3Sn_2-HT samples were obtained as single-phase products (the Supporting Information). In all cases, the lattice parameters determined from powder patterns and from single-crystal data agreed within standard deviations.

Single-crystal intensity data of $CaNi_4Sn_2$, $Ca_{0.5}Sr_{0.5}Ni_4Sn_2$, and $SrNi_4Sn_2$ were collected at room temperature with a Stoe IPDS-IIT image plate diffractometer with graphite monochromatized $Mo_{K\alpha}$ (0.71073 Å) radiation in oscillation mode. The absorption correction was numerical.[21,22] All relevant crystallographic data for the data collection and evaluation are listed in Table 1.

The single crystals were analyzed with a JEOL SEM 5900 LV scanning electron microscope. No impurity elements heavier than sodium were observed. The analysis revealed its composition (in atomic percentages) as: 14.5 (Ca), 56.1 (Ni), 29.4 (Sn) for $CaNi_4Sn_2$; 7.2 (Ca), 6.6 (Sr), 55.0 (Ni), 31.2 (Sn) for $Ca_{0.5}Sr_{0.5}Ni_4Sn_2$; and 11.9 (Sr), 59.1 (Ni), 29.0 (Sn) for $SrNi_4Sn_2$, which correspond to $Ca_{1.0(1)}Ni_{3.9(3)}Sn_{2.1(1)}$, $Ca_{0.5(1)}Sr_{0.5(1)}Ni_{3.8(3)}Sn_{2.2(2)}$, and $Sr_{0.8(1)}Ni_{4.1(3)}Sn_{2.1(1)}$, thus within standard deviations to the 1:4:2 compositions, obtained from the X-ray crystal structure analysis.

Careful analyses of the data set revealed a tetragonal Laue symmetry 4/*mmm* and the systematic extinctions led to the possible space groups *I*4/*mcm*, *I*4*cm*, and *I*$\bar{4}$*c*2, of which the group with the highest symmetry was found to be correct during the structure refinement. The starting atomic parameters for $SrNi_4Sn_2$ were deduced from an automatic interpretation of direct methods with SHELXS-97.[23] The atomic parameters of $SrNi_4Sn_2$ were taken as starting values for $CaNi_4Sn_2$. The structures were successfully refined with SHELXL-97[24] (full-matrix least-squares on F^2) with anisotropic atomic displacement parameters for all atoms. As a check for the correct composition and site assignment, the occupancy parameters were refined in a separate series of least-squares cycles along with the displacement parameters. All sites were fully occupied within two standard deviations and in the final cycles the ideal occupancies were assumed again. Final difference Fourier syntheses revealed no significant residual peaks. The positional parameters and interatomic distances of the refinement are listed in Table 2 and Table 3.

The structures of the new stannides are very closely related to $RENi_4Sn_2$ structures (RE=La, Ce, Pr, Nd, Sm),[25] which crystallize in the noncentrosymmetric space group *I*$\bar{4}$*c*2 of the KAu_4Sn_2-type.[26] In contrast to those structures, refinement converged well in the present case using the highest symmetry group *I*4/*mcm*. The structure refinement was also performed in the *I*$\bar{4}$*c*2 space group; however, the observed Flack parameter[27,28] and higher *R* values indicated that this space group was incorrect. The enhanced standard uncertainty of the Flack parameter results from

the low anomalous scattering contribution (light elements). A centrosymmetric structure was recently reported for AAu_4In_2 (A = K, Rb).[29]

Further details of the crystal structure investigation may be obtained from the Fachinformationzentrum Karlsruhe, 76344 Eggenstein-Leopoldshafen, Germany (E-mail: crysdata@fiz-karlsruhe.de) on quoting the depository numbers CSD-418131 ($SrNi_4Sn_2$), CSD-418132 ($Ca_{0.5}Sr_{0.5}Ni_4Sn_2$), and CSD-418133 ($CaNi_4Sn_2$).

Catalysis: Catalytic testing of the samples in the hydrogenation of citral was carried out in a high-pressure batch reactor described earlier.[30] The reactor was filled with the powdered samples. After addition of a solution of citral (1 mL, 47% *cis*-citral, 53% *trans*-citral) to *n*-hexane (9 mL), the reactor was stirred (850 rpm), purged with argon, and heated to 453 K. The reaction was started by the addition of hydrogen into the reactor. The process was stopped after a reaction time of 150 min. The product composition was determined by GC analysis (HP 6890, flame ionization detector, DB-WAX capillary column).

Calculations: The electronic structure was investigated with the local density-functional approach and the linear muffin-tin orbital (LMTO) method in the atomic sphere approximation (ASA), using the tight-binding (TB) program TB-LMTO-ASA.[31] The chemical bonding analysis was based on electronic density of states (DOS) curves, full-potential charge-density plots, and crystal-orbital Hamilton populations (COHPs).[32] A COHP plot shows DOS curves that are weighted by the contributions of each crystal orbital to some measure of the strength of a given bond. In a COHP analysis, it is the contribution of the covalent part of a particular interaction to the total bonding energy of the crystal. All COHP curves are presented here in the following format: positive values are bonding, and negative are antibonding. The basis set of short-ranged[33] atom-centered TB-LMTOs contained s-f valence functions for Sr and Sn and s-d valence functions for Ca and Ni. Ca 4p, Sr 5p, 4f, and Sn 5d and 4f orbitals were included using a downfolding technique.

Acknowledgement

This work was financially supported by the Deutsche Forschungsgemeinschaft (project numbers FA 198/4–1 and CL 168/3–1).

[1] a) G. C. Bond, Catalysis by Metals, Academic Press, New York, **1962**; b) C. Gieck, T. F. Fässler, S. Cavet, P. Claus, *Z. Anorg. Allg. Chem.* **2004**, *630*, 1724; c) J. Greeley, J. K. Nørskov, M. Mavrikakis, *Ann. Rev. Phys. Chem.* **2002**, *53*, 319; d) J. H. Sinfelt, *Proc. Am. Philos. Soc.* **1999**, *143*, 388.
[2] P. Claus, F. Raif, S. Cavet, S. Demirel-Gülen, J. Radnik, M. Schreyer, T. Fässler, *Catal. Commun.* **2006**, *7*, 611.
[3] C. Gieck, M. Schreyer, T. F. Fässler, S. Cavet, P. Claus, *Chem. Eur. J.* **2006**, *12*, 1924.
[4] P. Villars, *Pearson's Handbook, Desk Edition, Crystallographic Data for Intermetallic Phases*, American Society for Metals, Materials Park, OH, **1997**.
[5] D. A. Vennos, M. E. Badding, F. J DiSalvo, *J. Less-Common Met.* **1991**, *175*, 339.
[6] a) W. Dörrscheidt, H. Schäfer, *J. Less-Common Met.* **1978**, 58, 209; b) V. Hlukhyy, T. F. Fässler, *Inorg. Chem.* **2006**, *45*, 7408.
[7] A. Dascoulidou, F. Schucht, W. Jung, H. U. Schuster, *Z. Anorg. Allg. Chem.* **1998**, *624*, 119.
[8] A. Dascoulidou, P. Müller, W. Bronger, *Z. Anorg. Allg. Chem.* **1998**, *624*, 124.
[9] W. Dörrscheidt, N. Niess, H. Schaefer, *Z. Naturforsch. B* **1976**, *31*, 890.
[10] N. May, H. Schäfer, *Z. Naturforsch. B* **1974**, *29*, 20.
[11] A. K. Ganguli, J. D. Corbett, *J. Solid State Chem.* **1993**, *107*, 480.
[12] G. Nuspl, K. Polborn, J. Evers, G. A. Landrum, R. Hoffmann, *Inorg. Chem.* **1996**, *35*, 6922.
[13] D. Kußmann, R.-D. Hoffmann, R. Pöttgen, *Z. Anorg. Allg. Chem.* **1998**, *624*, 1727.
[14] R.-D. Hoffmann, D. Kussmann, U. C. Rodewald, R. Pöttgen, C. Rosenhahn, B. D. Mosel: *Z. Naturforsch. B* **1999**, *54*, 709.
[15] M. Boudard, P. Bordet, H. Vincent, F. Audebert, *J. Alloys Compd.* **2004**, *372*, 121.
[16] M. Schlüter, A. Kunst, R. Pöttgen, *Z. Anorg. Allg. Chem.* **2002**, *628*, 2641.
[17] M. Schlüter, U. Häussermann, B. Heying, R. Pöttgen, *J. Solid State Chem.* **2003**, *173*, 418.
[18] V. Hlukhyy, R. Pöttgen, *Z. Anorg. Allg. Chem.* **2005**, *631*, 2997.
[19] V. Hlukhyy, T. F. Fässler, *Proc. 9th International Conference On Crystal Chemistry of Intermatallic Compounds* (L'viv, Ukraine), **2005**, p. 44.
[20] J. Rodríguez-Carvajal. Program FullProf.2k, Version 20. Laboratoire Leon Brillouin (CEA-CNRS), France, **2005**.
[21] X-RED (1.26)-Data Reduction Program. Stoe & Cie., Darmstadt (Germany), **2004**.
[22] X-SHAPE (2.05)-Crystal Optimization for Numerical Absorption Correction. Stoe & Cie., Darmstadt (Germany), **2004**.
[23] G. M. Sheldrick, SHELXS-97, Program for the Determination of Crystal Structures, University of Göttingen, Göttingen (Germany) **1997**.
[24] G. M. Sheldrick, SHELXL-97, Program for Crystal Structure Refinement, University of Göttingen, Göttingen (Germany) **1997**.
[25] R. V. Skolozdra, I. V. Yasnitskaya, L. G. Aksel'rud, L. P. Komarovskaya, *Inorg. Mater.* **1988**, *24*, 54.
[26] H. D. Sinnen, H. U. Schuster, *Z. Naturforsch. B* **1978**, *33*, 1077.
[27] H. D. Flack, G. Bernadinelli, *Acta Crystallogr. Sect. A* **1999**, *55*, 908.
[28] H. D. Flack, G. Bernadinelli, *J. Appl. Crystallogr.* **2000**, *33*, 1143.
[29] B. Li, J. D. Corbett, *J. Am. Chem. Soc.* **2006**, *128*, 12392.
[30] M. Lucas, P. Claus, *Chem. Ing. Tech.* **2001**, *73*, 252.
[31] M. van Schilfgarde, T. A. Paxton, O. Jepsen, O. K. Andersen, G. Krier, *Programm TB-LMTO 4.6*, Max-Planck-Institut Stuttgart (Germany) **1994**.
[32] R. Dronskowski, P. E. Blöchl, *J. Phys. Chem.* **1993**, *97*, 8617.
[33] O. K. Andersen, O. Jepsen, *Phys. Rev. Lett.* **1984**, *53*, 2571.
[34] J. Donohue, *The Structures of the Elements*, Wiley, New York (USA) **1974**.
[35] M. Schreyer, T. F. Fässler, *Solid State Sci.* **2006**, *8*, 793.
[36] L. Pauling, B. Kamb, *Proc. Natl. Acad. Sci.* (USA) **1986**, *83*, 3569.
[37] P. Rahlfs, *Metallwirtsch. Metallwiss. Metalltech.* **1937**, *16*, 640.
[38] P. Wollesen, W. Jeitschko, *J. Alloys Comp.* **1996**, *67*, 243.
[39] N. C. Baenziger, R. E. Rundle, A. I. Snow, A. S. Wilson, *Acta Crystallogr.* **1950**, *3*, 34.
[40] A. M. Guloy, J. D. Corbett, *Inorg. Chem.* **1996**, *35*, 2616.
[41] G. Bruzzone, *J. Less-Common Met.* **1971**, *25*, 361.
[42] P. Claus, Y. Önal, "Regioselective Hydrogenations" in *Handbook of Heterogeneous Catalysis, vol. 7* (Eds.: G. Ertl, H. Knözinger, F. Schüth, J. Weitkamp), Wiley-VCH, Weinheim, **2008**, p. 3308.

Received: October 2, 2007
Published online: February 20, 2008

